Catalysis Today 413-415 (2023) 113980

Contents lists available at ScienceDirect

Catalysis Today

journal homepage: www.elsevier.com/locate/cattod

Design and synthesis of TiO_2/Ti_3C_2 composites for highly efficient photocatalytic removal of acetaminophen: The relationships between synthesis parameters, physicochemical properties, and photocatalytic activity

Anna Grzegórska [a,*], Agnieszka Gajewicz-Skretna [b], Grzegorz Trykowski [c], Karol Sikora [d], Anna Zielińska-Jurek [a,*]

[a] Department of Process Engineering and Chemical Technology, Faculty of Chemistry, Gdańsk University of Technology, G. Narutowicza 11/12, 80-233 Gdańsk, Poland
[b] Laboratory of Environmental Chemoinformatics, Faculty of Chemistry, University of Gdansk, Wita Stwosza 63, 80-308 Gdansk, Poland
[c] Faculty of Chemistry, Nicolaus Copernicus University in Toruń, Gagarina 7, 87-100 Toruń, Poland
[d] Department of Inorganic Chemistry, Faculty of Pharmacy, Medical University of Gdańsk, Al. Gen. J. Hallera 107, 80-416 Gdańsk, Poland

ARTICLE INFO

Keywords:
Acetaminophen
Chemometrics
MXene
Photocatalysis
Ti_3C_2
TiO_2

ABSTRACT

In this study, we report the potential of TiO_2/Ti_3C_2 composite fabricated by oxidation of MXene for degradation of persistent organic pollutants. The effect of the synthesis conditions (time, temperature, and reaction environment) on the morphology, physicochemical properties, and photocatalytic activity was investigated. It was found that acetaminophen degradation was positively correlated with TiO_2 content in the composite structure. Furthermore, the findings confirmed that the synthesis reaction environment strongly influenced the obtained materials photocatalytic activity. The TiO_2/Ti_3C_2 composite obtained by solvothermal route in the presence of hydrochloric acid and ammonium fluoride exhibited the highest efficiency towards acetaminophen degradation than other composite materials, for which ACT removal reached 92 % within 60 min of irradiation under simulated solar light. The improved photocatalytic performance can be attributed to the presence of anatase-rutile polymorphs exposing highly active { 0 0 1} and { 1 0 1} facets coupled with MXene. Superoxide anion radicals and hydroxyl radicals played a major role in ACT degradation. Moreover, 3-hydroxyacetaminophen was detected as the first intermediate of ACT degradation, leading quickly to aromatic ring opening and production of aliphatic acids. Overall, this work provides an effective strategy for designing novel and efficient MXene-based photocatalysts for the degradation of emerging contaminants in water systems.

1. Introduction

Nowadays, pharmaceuticals belonging to the group of persistent organic pollutants represent a new water quality challenge, with still unknown long-term impacts on human health and ecosystems [1]. Acetaminophen (*N*-Acetyl-p-aminophenol), also known as paracetamol, is an analgesic and antipyretic drug commonly used worldwide and detected in wastewater and surface waters [2]. The annual consumption of ACT reaches 4–50 tons per million habitants; thus a high amount of this pharmaceutical may be excreted to the environment in the unchanged form or as its active metabolites [3]. Based on the studies performed from 1999 to 2018 in Latin America, the range of ACT concentration in wastewater treatment plants effluents reached 17.1–29, 200 ng/dm^3, while in surface waters 3–25,200 ng/dm^3 [4].

In this regard, one of the primary challenges that societies will face during the 21st century is improving water quality by reducing pollution, minimizing the release of hazardous chemicals, and halving the proportion of untreated wastewater using the fundamentals of green chemistry and green engineering processes. This speaks for the development of new advanced treatment technologies such as photocatalysis to deal with these kinds of contaminants and improve the quality of treated wastewater before being safely discharged into public water bodies or for reuse.

MXenes are a group of materials consisting of transition metal carbides, nitrides, or carbonitrides, characterized by hydrophilic surface, good electrical conductivity, and chemical stability, which were

* Corresponding authors.
E-mail addresses: anna.grzegorska@pg.edu.pl (A. Grzegórska), annjurek@pg.edu.pl (A. Zielińska-Jurek).

https://doi.org/10.1016/j.cattod.2022.12.011
Received 27 August 2022; Received in revised form 8 November 2022; Accepted 20 December 2022
Available online 22 December 2022

discovered in 2011 [5]. The general formula of MXenes is $M_{n+1}X_nT_x$ (n = 1–4), where M is a transition metal, X represents carbon or nitrogen, and T_x refers to surface terminations (-F,-O,-OH) [6]. A novel and promising direction is using MXenes in photocatalysis [7,8]. MXenes may act as co-catalysts, enhancing the adsorption of the pollutants on the surface, improving the charge carriers separation, photocatalyst stability, and increasing the light absorption range [9,10]. The photocatalytic hydrogen production, CO_2 reduction as well as dyes degradation was previously described in the literature [11–13]. However, nowadays, only a few studies focus on the application of MXene materials for the photocatalytic degradation of active pharmaceutical ingredients. Jiang et al. [14] reported the application of MXene-derived C-TiO_2/Bi_4NbO_8Cl for the removal of ciprofloxacin. Liu et al. [15] investigated the potential of Ti_3C_2/TiO_2/BiOCl for the degradation of tetracycline. In the study of Liu et al. [16] the CdS@Ti_3C_2 @TiO_2 was used for the removal of sulfachloropyridazine. Yang et al. [17] proposed the application of PDI/g-C_3N_4/TiO_2@Ti_3C_2 for the photocatalytic degradation of atrazine. Shahzad et al. [18] and Grzegórska et al. [19] reported the potential of TiO_2/Ti_3C_2 and Fe-TiO_2/Ti_3C_2 composites for photocatalytic degradation of carbamazepine.

Formation of heterojunction between TiO_2 and MXene compound -$Ti_3C_2T_x$ is a promising approach to improve charge carriers separation and thus photocatalytic efficiency. MXene may form a Schottky barrier at the MXene-semiconductor heterojunction and act as a reservoir of photogenerated electrons [8]. Furthermore, depending on the synthesis conditions, different morphologies of TiO_2 with exposed crystal facets may be produced by in-situ oxidation of the MXene surface [12]. Our previous work confirmed that the formation of { 1 0 1} and { 0 0 1} facets might be particularly important in efficient photocatalytic degradation [20]. Facet-engineered TiO_2 with "surface heterojunction" which connects reductive { 1 0 1} facets and oxidative { 0 0 1} facets may effectively separate the oxidation and reduction centers of TiO_2 [19,21]. Dominant { 0 0 1} facets have a high ability to trap the photogenerated holes, while the concentration of the photogenerated electrons occurs on the { 1 0 1} facets [22]. This suggests that not only the presence of selected facets but also the ratio between them may determine the degradation rate [23]. Therefore, crystal engineering is one of the key factors affecting the efficiency of photocatalytic reactions.

In this regard, the present work represents a comprehensive investigation of the various synthesis conditions of TiO_2/Ti_3C_2 composites: (i) hydrothermal in deionized water, (ii) solvothermal in HBF_4, (iii) solvothermal in NH_4F and HCl, and (iv) simple calcination, to improve the physicochemical properties and the photocatalytic activity. For the first time, the effect of the reaction environment on the preparation of TiO_2/Ti_3C_2 composites exposing different crystal facets and applied for photocatalytic degradation of acetaminophen under simulated solar light was studied in detail. The chemometric analyses were employed to determine the relationships between synthesis parameters, physicochemical properties, and photocatalytic activity. Furthermore, for the most active sample, the possible reaction mechanism and degradation pathway were proposed.

2. Experimental

2.1. Photocatalyst preparation

The $Ti_3C_2T_x$ was obtained by etching aluminum from Ti_3AlC_2 using 48 % HF at room temperature for 24 h. TiO_2/Ti_3C_2 composites were prepared by a solvothermal method in the presence of HBF_4 (series TiO_2/Ti_3C_2_HBF_4 samples). In a typical synthesis, 60 cm^3 of HBF_4 (0.1 M) was added to 0.4 g of $Ti_3C_2T_x$, sonicated for 10 min, and mixed for 30 min (in a temperature ranging from 140° to 220°C and time from 6 to 24 h). Furthermore, the TiO_2/Ti_3C_2 composite was also obtained in deionized (DI) water during solvothermal synthesis (TiO_2/Ti_3C_2(220,24)_H_2O sample) to study the effect of the synthesis environment on morphology and photocatalytic activity. In this regard, 0.4 g of $Ti_3C_2T_x$ was added to 60 cm^3 of DI water and sonicated for 10 min. Then the suspension was mixed for 30 min and transferred into a Teflon-lined stainless steel reactor. The reaction was performed at 220 °C for 24 h. Another sample of $Ti_3C_2T_x$ was calcined at 550 °C for 2 h with a heating rate of 2 °C/min (TiO_2/Ti_3C_2(550,2) sample). Finally, the $Ti_3C_2T_x$ sample was also treated during solvothermal synthesis in HCl with NH_4F solution (TiO_2/Ti_3C_2(220,24)_NH_4F_HCl sample). In this regard, 60 cm^3 of HCl (3 M) was mixed with 0.1 g NH_4F, and 0.4 g of $Ti_3C_2T_x$ was added to the above solution and sonicated for 10 min. Then the suspension was stirred for 30 min and transferred into a Teflon-lined stainless steel reactor. The reaction was performed at 220 °C for 24 h. All resulting material was rinsed with deionized water and dried in an oven at 50 ℃.

2.2. Materials characterization

The characterization methods applied in this work can be found in subsection 2.3. in Supporting Materials.

3. Results and discussion

3.1. Physicochemical characteristics of TiO_2/Ti_3C_2 composites prepared by a solvothermal method in the presence of HBF_4

In the first step of the study, the composite synthesis was optimized to correlate the morphological and physicochemical parameters with photocatalytic activity. Firstly, TiO_2/Ti_3C_2 composites were prepared by a solvothermal method in the presence of HBF_4 at a temperature ranging from 140 °C to 220 °C for 6–24 h, as presented in Table 1 (series A). The SEM and TEM analyses confirmed the formation of the accordion-like structure of $Ti_3C_2T_x$ (see Fig. 1a-b). The solvothermal reaction in HBF_4 led to the formation of decahedral anatase particles (DAPs) on the $Ti_3C_2T_x$ layer, as shown in Fig. 1c-f. Analyzing the SEM images of all prepared TiO_2/Ti_3C_2 composites, the diversity of sample morphology can be noticed. The samples TiO_2/Ti_3C_2(140,24) and TiO_2/Ti_3C_2(180,6) presented the initial stage of TiO_2 in-situ growing and formation. Meanwhile, the sample TiO_2/Ti_3C_2(180,24) showed the most uniform DAPs, equally distributed on the MXene layers. Other samples presented a size variety, with smaller and larger DAPs. The average length and height of DAPs were calculated based on the measurements of 50 particles for each sample from the SEM images and are summarized in Table 1.

The BET surface area increased with the increase in the reaction time and temperature, as presented in Table 1. However, this trend was observed only to a certain point. Prolonged reaction time and higher temperature caused a decrease in specific surface area. The CHN analysis of MXene showed that the sample contains about 8.49 % of carbon and 2.15 % of hydrogen (as shown in Table 1S). The XRD analysis, presented in Fig. 1S in Supporting Materials, confirmed the successful etching of aluminum from the Ti_3AlC_2. For the obtained MXene materials, the characteristic diffraction peaks at $2\theta = 8.8°$, 18.1°, and 27.4° corresponding to (002), (004), and (006) planes were noticed. Furthermore, the Rietveld analysis of XRD patterns revealed that samples TiO_2/Ti_3C_2(140,6), TiO_2/Ti_3C_2(140,12), TiO_2/Ti_3C_2(160,6) are pure MXene or contain a very low content of TiO_2 because any signals corresponding to TiO_2 were not observed. Furthermore, the Rietveld analysis confirmed an increase of TiO_2 content in the composite with an increase in time and temperature. The highest content of TiO_2 was noticed for sample TiO_2/Ti_3C_2(220,48) with almost 100 % of TiO_2 and sample TiO_2/Ti_3C_2(220,24) containing 99.8 % of TiO_2 and 0.2 % of MXene.

To confirm the presence of MXene in the sample TiO_2/Ti_3C_2(220,24), the additional STEM-EDX-EELS analysis was performed. As presented in Fig. 2S in Supporting Materials for sample TiO_2/Ti_3C_2(220,24) two different areas may be distinguished. The first one with higher carbon content indicates the presence of $Ti_3C_2T_x$, and the second with negligible carbon content is TiO_2.

Table 1
Physicochemical characteristics and photocatalytic activity of TiO_2/Ti_3C_2 composites.

Sample	Synthesis conditions		BET surface area (m^2/g)	Anatase (101) crystallite size (nm)	Composition (%)		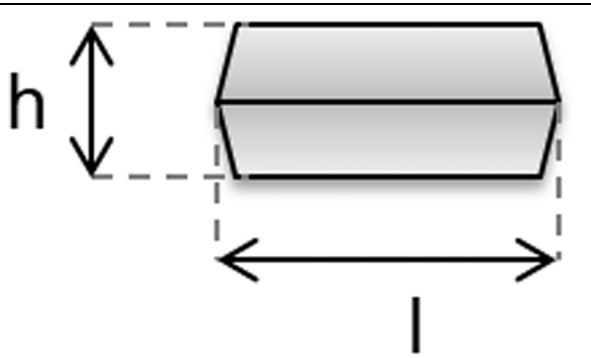		Acetaminophen degradation rate constant ($min^{-1} \cdot 10^{-2}$)
	Temperature (℃)	Time (h)			TiO_2	Ti_3C_2	h (nm)	l (nm)	
$Ti_3C_2T_x$	25	24	7.5	nd	0	100	nd	nd	0.2 ± 0.02
TiO_2/Ti_3C_2(140,6)	140	6	8.4	nd	0	100	nd	nd	0.22 ± 0.01
TiO_2/Ti_3C_2(140,12)	140	12	9.5	nd	0	100	nd	nd	0.24 ± 0.01
TiO_2/Ti_3C_2(140,24)	140	24	12.9	19	11.5	88.5	nd	nd	1.01 ± 0.03
TiO_2/Ti_3C_2(160,6)	160	6	9.9	nd	0	100	nd	nd	0.28 ± 0.01
TiO_2/Ti_3C_2(160,12)	160	12	16.0	27	18.6	81.4	35	140	1.66 ± 0.04
TiO_2/Ti_3C_2(160,24)	160	24	24.8	24	45.8	54.2	52	268	1.89 ± 0.02
TiO_2/Ti_3C_2(180,6)	180	6	16.3	24	13.5	86.5	nd	nd	0.99 ± 0.03
TiO_2/Ti_3C_2(180,12)	180	12	24.0	38	42.4	57.6	45	184	2.04 ± 0.02
TiO_2/Ti_3C_2(180,24)	180	24	21.5	40	81.7	18.3	71	328	1.22 ± 0.03
TiO_2/Ti_3C_2(200,6)	200	6	24.2	35	31.6	68.4	44	117	1.14 ± 0.03
TiO_2/Ti_3C_2(200,12)	200	12	23.0	41	69.8	30.2	64	201	1.24 ± 0.02
TiO_2/Ti_3C_2(200,24)	200	24	17.2	34	98.8	1.2	76	214	1.03 ± 0.01
TiO_2/Ti_3C_2(220,6)	220	6	22.4	41	63.9	36.1	96	289	1.37 ± 0.03
TiO_2/Ti_3C_2(220,12)	220	12	16.5	27	85.9	14.1	121	142	0.99 ± 0.02
TiO_2/Ti_3C_2(220,24)	220	24	10.0	34	99.8	0.2	88	114	2.86 ± 0.03
TiO_2/Ti_3C_2(220,48)	220	48	8.5	38	100	0	79	101	2.49 ± 0.02

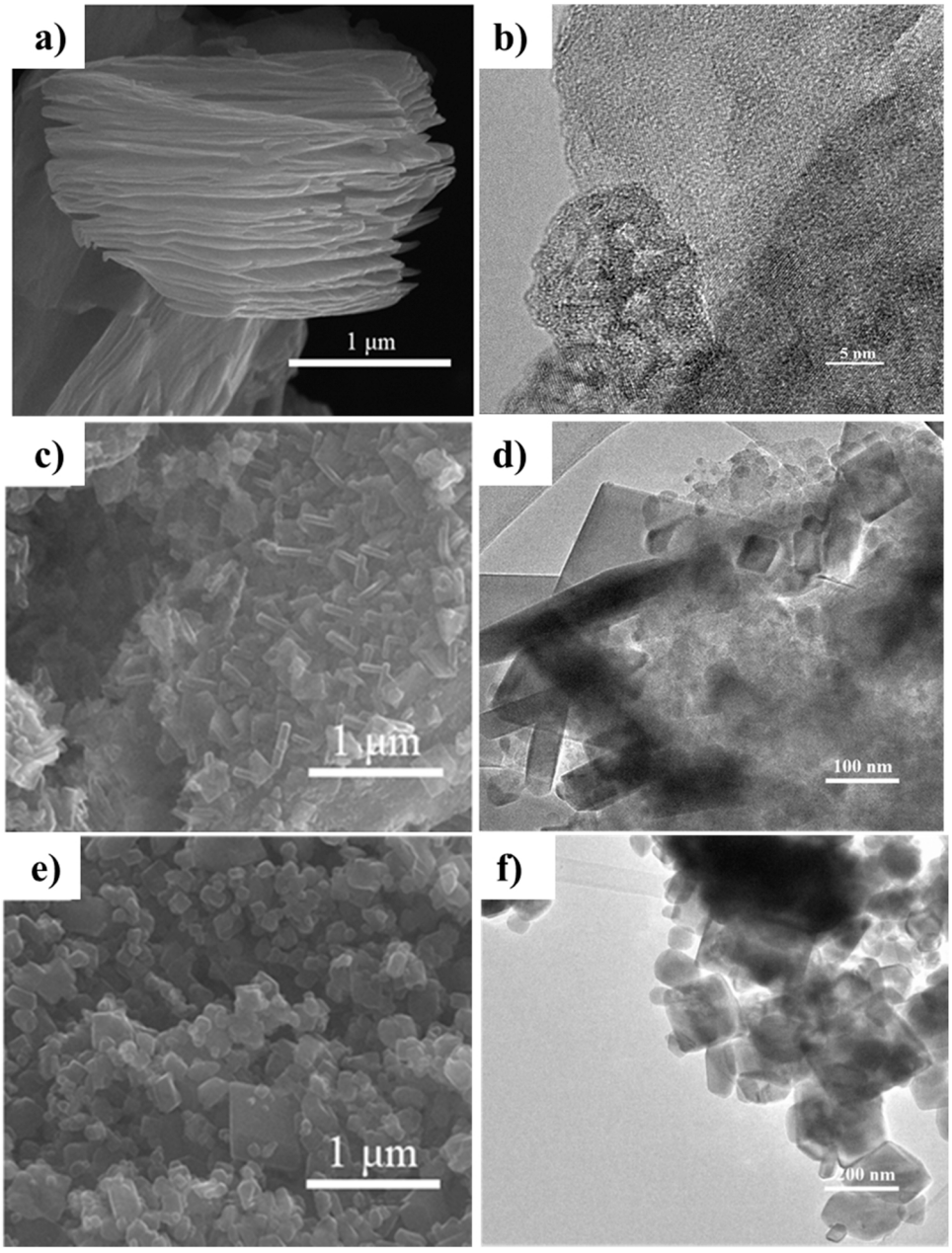

Fig. 1. The SEM and TEM images for Ti_3C_2 (a,b), TiO_2/Ti_3C_2 composite synthesized at 180 °C (c,d) and 12 h, TiO_2/Ti_3C_2 composites synthesized at 220 °C and 24 h (e,f).

In order to catch possible (dis)similarities among TiO_2/Ti_3C_2 composites, find hidden patterns in data and determine the causal relationships between the photocatalytic performance of TiO_2/Ti_3C_2 composites and the samples morphology, physicochemical properties as well as synthesis conditions, the chemometric analyses were carried out.

The tree-like graph is shown in Fig. 3S in Supporting Materials. Since the circular dendrogram for the hierarchical cluster analysis (HCA) does not identify the causal relationship between variables, hence to gain an overall idea of which MXene morphological features, physicochemical properties and/or synthesis conditions are significantly related to the enhanced photocatalytic performance of the TiO_2/Ti_3C_2 composites, the Principal Component Analysis (PCA) analysis was performed.

PCA discovers interpretable patterns and trends in the data that cannot be captured by a human eye and simultaneously simplifies the complexity in high-dimensional data. This is done by finding the orthogonal projections that maximize the variance of the data, known as the principal components (PCs). Principal components as linear combinations of the original variables (here: morphological features, physicochemical properties and/or synthesis conditions of MXene) are extracted in a way that the first principal component (PC1) explains as much variance in the original data as possible and each subsequent principal component accounts for less and less variance. Following the Kaiser criterion that states that meaningful are only those components with eigenvalues equal or higher than one, the first two principal components (PC1 and PC2) were retained for further analysis. Together, the first two PCs contain 84.83 % (62.96 % + 21.87 %) of the information (variances) contained in the data. The projection of the data onto the subspace spanned by PC1 and PC2 is shown in Fig. 2a, known as a biplot. To gain mechanistic insights into the efficiency of TiO_2/Ti_3C_2 composites towards acetaminophen degradation, the analysis of the normalized factor loadings was carried out (Fig. 2b). These loadings are, by definition, correlations between the original variables and the PCs.

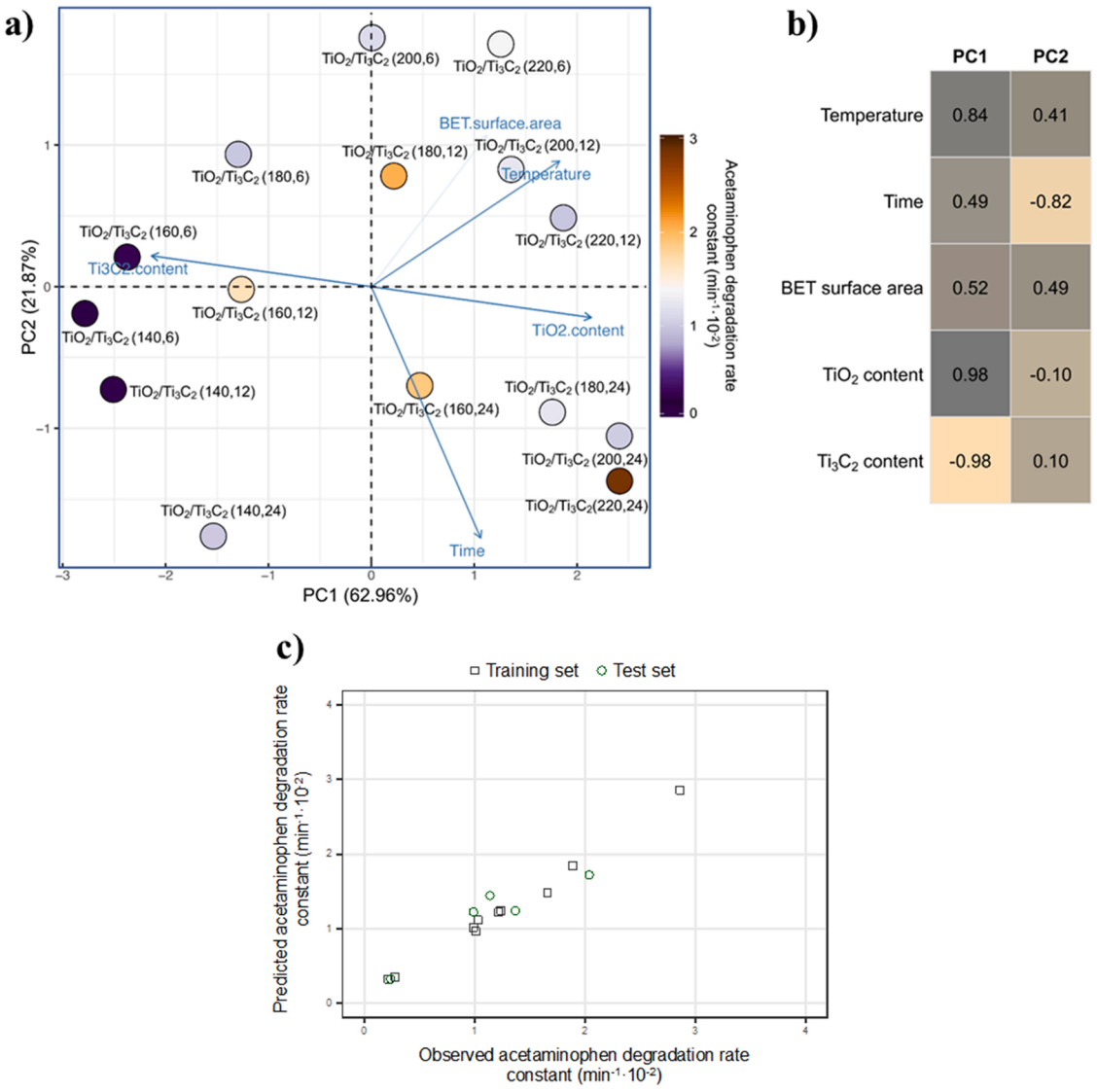

Fig. 2. (a) The PCA biplot of the first two principal components (PC1-PC2) that illustrates the grouping of TiO_2/Ti_3C_2 composites (points) in the space of explanatory variables (vectors). The color of each data point represents the value of the acetaminophen degradation rate constant ($min^{-1}\cdot10^{-2}$): dark purple means the lowest value of the photocatalytic activity, whereas dark brown – the highest photocatalytic activity; (b) The plot of normalized factor loadings utilized for providing a physical interpretation of principal components, (c) The plot of experimentally observed versus predicted values of acetaminophen degradation rate constant in the presence of TiO_2/Ti_3C_2 composites ($min^{-1}\cdot10^{-2}$). (For interpretation of the references to color in this figure legend, the reader is referred to the web version of this article.)

They quantify the extent of the relevance of original variables in explaining a given principal component. According to the so-called Malinowski rule, the statistically significant ones are only those which have absolute values equal to or higher than 0.7. A closer look at Fig. 2b reveals that the variables with the greatest influence on the first principal component (PC1) are the content of TiO_2 and the content of Ti_3C_2, followed by synthesis temperature.

The projection of the samples onto the PCs showed that the samples with the lowest photodegradation rate constant (below 0.3 $min^{-1}\cdot10^{-2}$) are furthest apart from the other composites and are located on the left side of the biplot. It is straightforward to see that these nanocomposites have low PC1 scores (X-axis), which means they are characterized by low values of the positively correlated variables (i.e., TiO_2 content and temperature), and thereby by high values of the negatively correlated variable (i.e., Ti_3C_2 content). This observation is even more obvious in the light of disclosure that these composites are pure MXene without TiO_2. In addition, these samples are characterized by the lowest surface area compared to the other TiO_2/Ti_3C_2 nanocomposites. Examining the biplot further, one can see that the samples with the highest content of TiO_2 and the lowest content of MXene were placed on the right side of the biplot. These results suggest that the greatest distances between the nanocomposites are along PC1 (X-axis), expressed by the composition and corresponding contents of TiO_2 and Ti_3C_2.

Interestingly, the samples with a higher concentration of TiO_2 than that of Ti_3C_2 were placed on the right side of the biplot and showed the differentiation along PC2 (Fig. 2a). The interpretation of PC2 (Y-axis) which reflects the synthesis conditions of nanocomposites, is not so intuitive. It is strongly negatively correlated with reaction time. As seen in Fig. 2a, composites of low and moderate values of activity of acetaminophen degradation have both low and high PC2 scores. Although PC2 does not clearly distinguish between the samples with the higher and the lower activity of acetaminophen degradation, it can be seen that the photocatalytic performance of composites slightly increases, moving downwards along the Y-axis (PC2). This observation is in line with the correlogram analysis (Fig. 4S). The temperature is strongly positively correlated with TiO_2 content ($r = 0.81$), which implies that as

temperature increases, TiO_2 content also tends to increase. A correlation between BET surface area and Ti_3C_2 content, on the other hand, indicates a weak negative correlation ($r = -0.37$), meaning that, although an increase in the first variable will likely lead to decrease in the second variable, the relationship is not very strong. As seen in Fig. 4S, the acetaminophen degradation rate constant shows a positive correlation with TiO_2 content in the composite, reaction time, synthesis temperature and BET surface area and a negative correlation with Ti_3C_2 content.

The highest photocatalytic performance with the acetaminophen degradation rate constant equal to 2.86 ± 0.03 ($min^{-1} \cdot 10^{-2}$) was obtained by the TiO_2/Ti_3C_2(220,24) sample located on the right inferior half of the biplot (Fig. 2a). This sample is composed of TiO_2 (99.8 wt%) and Ti_3C_2 (0.2 wt%). With an increase of Ti_3C_2 content up to 36.1 wt%, the photocatalytic activity of TiO_2/Ti_3C_2 composites decreased sharply and was more than 50 % less compared to the photocatalytic performance of TiO_2/Ti_3C_2(220,24) sample (Table 1). Interestingly, further increasing the Ti_3C_2 content enhanced the photocatalytic performance and resulted in higher than expected values of acetaminophen degradation rate constants.

As seen from Fig. 2a, the second, the third and the fourth composites with the highest acetaminophen degradation rate constants TiO_2/Ti_3C_2(180,12), TiO_2/Ti_3C_2(160,24), and TiO_2/Ti_3C_2(160,12) were placed nearest from the biplot origin. The composition ratio of TiO_2 to Ti_3C_2 in these composites was 42.4: 57.6 wt%, 45.8: 54.2 wt% and 18.6: 81.4 wt%, respectively. Contrary to the TiO_2/Ti_3C_2(220,24) sample, these composites were obtained at lower temperatures and, additionally, two of them also in a shorter synthesis time. This might suggest that the photocatalytic performance of TiO_2/Ti_3C_2 nanocomposites can be greatly affected not only by the chemical composition of samples but also by other factors, such as synthesis conditions (i.e., temperature, reaction time).

Finally, the computer-aided (so-called *in silico*) modelling was additionally conducted to meet the research objectives of the study. As a logical extension of experimental research, *in silico* modelling identifies the essential parameters related to a target activity or molecular property (e.g., photocatalytic activity) and enables its prediction for untested compounds from experimental training data and suitable mathematical model. Hence, before model development, the dataset of 15 experimentally tested TiO_2/Ti_3C_2 nanocomposites was split into a training set of 10 samples and a test (external assessment) set of 5 samples using the sorted response-based division algorithm (in ascending order). Considering the limited size of the available dataset, the kernel-weighted local polynomial regression (KwLPR) approach [24,25], being a pointwise iterative method, was used for *in silico* model development. Likewise, in the case of other similarity-based modelling methods, the KwLPR approach seeks to estimate the unknown regression function point by point. This means that the KwLPR algorithm approximates the (unknown) posterior molecular property using only a small fraction of the training data points that lie in the local neighbourhood of each point of estimate. It does this by fitting a polynomial at each point in the dataset to a certain (user-defined) number of k nearest neighbours, whose explanatory variables values are similar to the point of estimation. The polynomial is obtained in the distance weighted least square estimation, which allows to allocate more weight to the points near the target point being estimated and less weight to the points further away. The weights reflecting the relative importance/contribution of each of the k neighbours according to their distance to the target point are used then to estimate a weighted least squares regression local model. Finally, the regression function (i.e., local model) is applied to compute the value of a point estimate.

In this study, the best estimator's parameters that control the size and the shape of the neighbourhood (i.e., the bandwidth), the local weights (i.e., the kernel function) and the flexibility of the regression function (i.e., the degree of the local polynomial used for smoothing) were obtained through the leave-one-out validation process. To evaluate both aleatoric and epistemic uncertainty of a developed *in silico* model, i.e., to verify how well the model does fit to the training dataset and predict the activity of unseen data (outside the training set), various quality metrics were computed. The goodness-of-fit of a model was ascertained by the determination coefficient (R^2), and the root means a square error of calibration ($RMSE_C$). While the true predictive performance of the model was examined with external validation coefficients (Q^2_{F1}, Q^2_{F2}, Q^2_{F3}), concordance correlation coefficient (CCC), and root means a square error of prediction ($RMSE_P$) [26–28].

In accordance with our expectations, the chemical composition of the composite nanomaterials is not sufficient to reflect variations in the acetaminophen degradation rate constant. The overall quality metrics of such a model were disappointing (i.e., R^2, $Q^2_{F1\text{-}F3} < 0.70$) and did not meet the commonly accepted requirements of *in silico* model. To improve the model performance and shed light on the mechanism driving acetaminophen degradation in the presence of TiO_2/Ti_3C_2 composites, the model was enriched with the synthesis conditions (i.e., with either synthesis temperature or synthesis time). Both refined models appeared to be more efficient and reliable compared to the original model (i.e., R^2, $Q^2_{F1\text{-}F3} > 0.70$). Interestingly, the model linking the acetaminophen degradation rate constant with the mass ratio of TiO_2 to Ti_3C_2 and synthesis temperature posed a better model's performance than the model using synthesis time as the explanatory variable. This can be explained by the slightly greater strength of the relationship between acetaminophen degradation rate constant and synthesis temperature ($r = 0.49$) than between acetaminophen degradation rate constant and synthesis time ($r = 0.46$) (Fig. 2b). Detailed information on the final model tuning parameters, including the kernel function applied, the calculated bandwidth for both explanatory variables, as well as the model's quality metrics, is provided in Table 2S in Supporting Materials. The analysis of the statistical metrics confirmed that the model demonstrated excellent fitting ability and external predictive power (i.e., generalization capabilities). This conclusion is clearly supported by a visual analysis of the scatter plot between the observed and predicted values of the acetaminophen degradation rate constant, shown in Fig. 2c.

As can be seen from the graph, the majority of the data points are clustered tightly around the best fit line, indicating high (close to 1) values of R^2 and Q^2. Since the developed KwLPR model fulfilled all stringent quality criteria, it has been utilized to predict the photocatalytic performance for a set of eight new TiO_2/Ti_3C_2 nanocomposites for which the experimental data have been unavailable up to now (Table 3S). The reliability of the predictions for these new composites will be subject to further experimental investigation.

3.2. The effect of reaction environment on TiO_2/Ti_3C_2 composites physicochemical properties and photocatalytic activity

In order to compare the impact of the reaction environment on the photocatalytic activity, the best parameters of the solvothermal synthesis in HBF_4 (series A, TiO_2/Ti_3C_2(220,24) sample) were applied for the preparation of the TiO_2/Ti_3C_2 composites in deionized water (TiO_2/Ti_3C_2(220,24)_H_2O sample) and in HCl and NH_4F (TiO_2/Ti_3C_2(220,24)_NH_4F_HCl sample). Furthermore, TiO_2/Ti_3C_2 nanocomposite was also obtained during the calcination of Ti_3C_2 (TiO_2/Ti_3C_2(550,2) sample) in airflow at 550 °C for 2 h (optimized calcination temperature in the range 350–650 °C).

Firstly, a comparison of structural and textural properties for the obtained TiO_2/Ti_3C_2 composites was performed. The XRD diffractograms for TiO_2/Ti_3C_2 samples synthesized at various conditions are shown in Fig. 5Sa. The diffraction patterns of TiO_2/Ti_3C_2(220,24)_HBF_4 and TiO_2/Ti_3C_2(550,2) are highly similar and correspond to the anatase phase. In the case of sample TiO_2/Ti_3C_2(220,24)_H_2O, the peaks at 8.9 ° and 18.3 ° correspond to the presence of MXene, while a minority of the rutile phase can be observed at 27.5°. For TiO_2/Ti_3C_2(220,24)_NH_4F_HCl, the characteristic signals at 25.2 ° and 27.3 °, corresponding to the (001) plane of anatase and (110) plane of rutile were

distinguished. In contrast to TiO_2/Ti_3C_2(220,24)_H_2O, the sample TiO_2/Ti_3C_2(220,24)_NH_4F_HCl is a composition of rutile (73.7 %) with a minority of anatase (26.3 %). Similar, Li and Gray [29] observed the formation of mixed-phase titanium (IV) oxide in the presence of hydrochloric acid when titanium tetra-isopropoxide was used as the titanium precursor. Furthermore, it was observed that halide ions enhanced the anatase-to-rutile phase transition [30]. The average size of anatase and rutile crystallites for TiO_2/Ti_3C_2 composites are summarized in Table 4S, while lattice parameters in Table 5S.

The DR/UV–vis spectra of the prepared composites are shown in Fig. 5Sb. The prepared samples showed absorption characteristics typical to anatase, with an absorption edge of about 400 nm extended to vis range due to $Ti_3C_2T_x$ presence. For the sample, TiO_2/Ti_3C_2(220,24)_H_2O with higher content of $Ti_3C_2T_x$, the increased absorption from 600 nm to 800 nm can be observed.

Comparing the composite morphology (Fig. 6S) it can be noticed that sample TiO_2/Ti_3C_2(220,24)_HBF_4 contains various size DAPs with the lowest surface area, about 10.0 m^2/g. For sample TiO_2/Ti_3C_2(220,24)_H_2O synthesized in the pure DI water, Ti_3C_2 sheets were covered by densely packed and irregularly shaped TiO_2 particles with the highest surface area of about 26.4 m^2/g among all prepared samples. Meanwhile, analyzing the SEM images of TiO_2/Ti_3C_2(550,2) it can be noticed that the agglomerated crystals were connected to each other to form a net shape. The sample TiO_2/Ti_3C_2(220,24)_NH_4F_HCl was a mixture of various size decahedral and octahedral TiO_2 particles exposing { 1 0 1} and { 0 0 1} facets.

The XPS analyses were performed to study the chemical states of photocatalysts surface composition, and the results are shown in Fig. 7S. The Ti 2p peak can be deconvoluted in three pairs of the doublet with peaks at 455 eV, 457 eV, and 459 eV (Ti 2p 3/2) assigned to Ti-C, substoichiometric TiC_x ($x < 1$), or titanium oxycarbides and TiO_2, respectively. However, for sample TiO_2/Ti_3C_2(550,2), notable differences from other samples can be observed. The main peak instead of TiO_2 was attributed to Ti^{3+} (457 eV), which may indicate the formation of Ti ions with a reduced charge state (Ti_xO_y). Similar phenomena were observed by Kong et al. [31] for Ti_3C_2 calcined at 700 °C. For all materials, the C1s spectra consist of five signals at 283 eV, 283.5 eV, 285 eV, 286.7 eV, and 288.5 eV assigned to Ti-C, C-Ti-O, adventitious carbon, C-O, and C-F bonds, respectively. Meanwhile, O1s signal may be deconvoluted into four signals at 528.5 eV, 530 eV, 531.5 eV, and 532.5 eV, corresponding to Ti-O-Ti, Ti-OH, C-O, and C═O.

Finally, the comparison of photocatalytic activity of the MXene-derived TiO_2/Ti_3C_2 composites prepared in different reaction environments is presented in Fig. 3a. The pure Ti_3C_2 compound showed negligible ACT photocatalytic removal. Similar very low photocatalytic activity for pure MXene was confirmed in previous studies [11,32,33]. However, in the TiO_2/Ti_3C_2 composite, MXene may act as a reservoir of photogenereted electrons and thus decrease the electron-hole recombination [34]. The highest rate constant is observed for TiO_2/Ti_3C_2(220,24)_NH_4F_HCl composite. This indicates that the bi-phase anatase-rutile structure of TiO_2 exposing highly active { 0 0 1} and { 1 0 1} facets greatly improved the photocatalytic degradation of acetaminophen. The photocatalytic activity increase can also be attributed to the morphological properties of TiO_2 consisting of decahedral and octahedral particles compared to other morphologies observed for samples obtained in different conditions. Meanwhile, sample TiO_2/Ti_3C_2(550,2) showed the lowest photocatalytic activity towards ACT degradation. This may be related to the morphology and highly defective (Ti^{3+} centers) surface of the photocatalyst. Previous studies also proved that excess defects would form the recombination center and be adverse to the separation of the charge carriers [35]. Furthermore, based on the trapping experiment in the presence of scavengers, it was noticed that the major reactive oxygen species responsible for ACT degradation are superoxide anion radicals and hydroxyl radicals (Fig. 3b).

Based on the Mott-Schottky analysis (Fig. 8S) it can be concluded that TiO_2/Ti_3C_2(220,24)_NH_4F_HCl composite showed typical characteristics for n-type semiconductor. The potential of flat band edge position was recorded at − 0.9 V vs. Ag/AgCl and converted to a value of − 0.61 V vs. NHE. According to band gap energy equal 2.8 eV the valence band (VB) edge of the composite was determined as approx. 2.19 eV. vs NHE. The proposed mechanism of acetaminophen degradation with TiO_2/Ti_3C_2(220,24)_NH_4F_HCl material is presented in the Fig. 3c. Photogenerated electrons in TiO_2 may be transferred to MXenes at the interface due to the higher potential of MXenes and inhibit recombination of photogenerated electron–hole pairs. Therefore, Ti_3C_2 may enhance the efficiency of charge separation and contribute to improved photocatalytic activity.

The proposed pathway of ACT degradation is presented in Fig. 3d. According to the LC-MS analyses, 3-hydroxyacetaminophen was detected as the first main intermediate of ACT decomposition, which suggests that hydroxylation of the benzene ring was a primary step of the degradation pathway. Moreover, based on the obtained results, 3-hydroxyacetaminophen quickly degraded within time and was further transformed through benzene ring cleavage to aliphatic acids [36,37].

Furthermore, the photocatalytic activity of the most active TiO_2/Ti_3C_2(220,24)_NH_4F_HCl composite was compared with the recently reported photocatalysts applied for photodegradation of ACT and the data are summarized in Table 6S. It was found that the photocatalyst prepared in our work has excellent performance compared with other materials with high degradation efficiency of ACT degradation within 60 min under simulated solar light.

4. Conclusions

In summary, the prepared TiO_2/Ti_3C_2 composites show good potential for photocatalytic water treatment. Based on the chemometric analyses, the photocatalytic activity was found to be significantly varied from the synthesis conditions. Chemometric analyses revealed that ACT degradation shows a positive correlation with TiO_2 content in the composite, reaction time, synthesis temperature, and BET surface area. The highest activity in this series was observed for the sample synthesized at 220 °C for 24 h. This work also demonstrates the effect of the synthesis environment on physicochemical properties and photocatalytic activity. In particular, the TiO_2/Ti_3C_2(220,24)_NH_4F_HCl displays improved photocatalytic efficiency than other composites towards ACT degradation under simulated solar light (92 % within 60 min). This phenomenon may be attributed to the formation anatase-rutile polymorphs exposing highly active { 1 0 1} facets and {0 0 1} facets coupled with MXene. Additionally, the photocatalytic mechanism was elucidated according to the band-gap energy, Mott Schottky plot and the trapping experiment. It was revealed that the main reactive oxygen species participating in photodegradation process are $\cdot O_2^-$ and ·OH. Furthermore, based on the LC/MS analyses, 3-hydroxyacetaminophen was detected as the first intermediate of photocatalytic process, and a possible degradation pathway was proposed.

Funding

The research was financially supported by Polish National Science Centre (Grant No. NCN 2018/30/E/ST5/00845.

CRediT authorship contribution statement

Anna Grzegórska: Formal analysis, Investigation, Methodology, Writing – original draft, Writing – review & editing. **Agnieszka Gajewicz-Skretna:** Formal analysis, Methodology. **Anna Zielińska-Jurek:** Conceptualization, Methodology, Resources, Supervision, Project administration,Funding acquisition, Writing – original draft, Writing – review & editing. **Grzegorz Trykowski**: Formal analysis. **Karol Sikora**: Formal analysis.

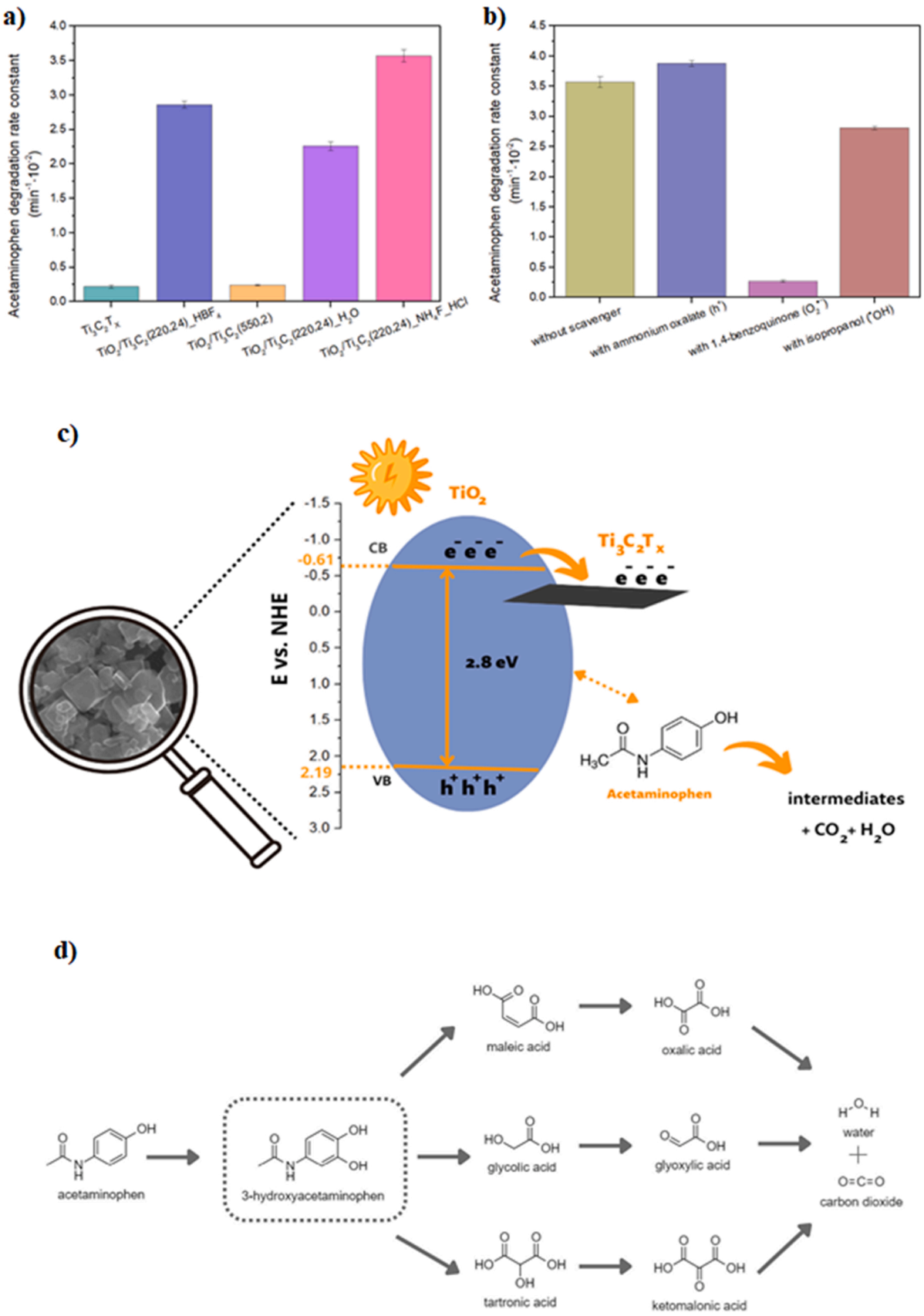

Fig. 3. The acetaminophen degradation for TiO_2/Ti_3C_2 composites (a), acetaminophen degradation with scavengers (b), proposed mechanism of ACT degradation (c), and proposed degradation pathway (d) for TiO_2/Ti_3C_2(220,24)_NH_4F_HCl.

Declaration of Competing Interest

The authors declare that they have no known competing financial interests or personal relationships that could have appeared to influence the work reported in this paper.

Data availability

Data will be made available on request.

Acknowledgements

This research was financially supported by the Polish National Science Centre (grant no. NCN 2018/30/E/ST5/00845).

Appendix A. Supporting information

Supplementary data associated with this article can be found in the online version at doi:10.1016/j.cattod.2022.12.011.

References

[1] J. Rivera-Utrilla, M. Sánchez-Polo, M.Á. Ferro-García, G. Prados-Joya, R. Ocampo-Pérez, Chemosphere 93 (2013) 1268–1287, https://doi.org/10.1016/j.chemosphere.2013.07.059.
[2] Y. Ishitsuka, Y. Kondo, D. Kadowaki, Biol. Pharm. Bull. 43 (2020) 195–206, https://doi.org/10.1248/bpb.b19-00722.
[3] R.A. Moore, N. Moore, Eur. J. Hosp. Pharm. 23 (2016) 187–188, doi.org/10.1136/ejhpharm-2016-000952.
[4] C. Peña-Guzmán, S. Ulloa-Sánchez, K. Mora, R. Helena-Bustos, E. Lopez-Barrera, J. Alvarez, M. Rodriguez-Pinzón, J. Environ. Manag. 237 (2019) 408–423, https://doi.org/10.1016/j.jenvman.2019.02.100.
[5] M. Naguib, M. Kurtoglu, V. Presser, J. Lu, J. Niu, M. Heon, L. Hultman, Y. Gogotsi, M.W. Barsoum, Adv. Mater. 23 (2011) 4248–4253, https://doi.org/10.1002/adma.201102306.
[6] P. Urbankowski, B. Anasori, T. Makaryan, D. Er, S. Kota, P.L. Walsh, M. Zhao, V. B. Shenoy, M.W. Barsoum, Y. Gogotsi, Nanoscale 8 (2016) 11385–11391, https://doi.org/10.1039/c6nr02253g.
[7] P. Kuang, J. Low, B. Cheng, J. Yu, J. Fan, J. Mater. Sci. Technol. 56 (2020) 18–44, https://doi.org/10.1016/j.jmst.2020.02.037.
[8] Q. Zhong, Y. Li, G. Zhang, Chem. Eng. J. 409 (2021), 128099, https://doi.org/10.1016/j.cej.2020.128099.
[9] L. Cheng, X. Li, H. Zhang, Q. Xiang, J. Phys. Chem. Lett. 10 (2019) 3488–3494, https://doi.org/10.1021/acs.jpclett.9b00736.
[10] J. Peng, X. Chen, W.J. Ong, X. Zhao, N. Li, Chem 5 (2019) 18–50, https://doi.org/10.1016/j.chempr.2018.08.037.
[11] M. Tahir, Energy Fuels 35 (2021) 14197–14211, https://doi.org/10.1021/acs.energyfuels.1c01340.
[12] A.A. Khan, M. Tahir, Z.Y. Zakaria, J. Environ. Chem. Eng. 9 (2021), 105244, https://doi.org/10.1016/j.jece.2021.105244.
[13] M. Tahir, A. Sherryna, R. Mansoor, A.A. Khan, S. Tasleem, B. Tahir, ACS Appl. Nano Mater. 5 (2022) 18–54, https://doi.org/10.1021/acsanm.1c03112.
[14] D. Jiang, X. Sun, X. Wu, S. Zhang, X. Qu, L. Shi, Y. Zhang, F. Du, Nanophotonics 9 (2020) 2077–2088, https://doi.org/10.1515/nanoph-2020-0088.
[15] H. Liu, C. Yang, X. Jin, J. Zhong, J. Li, Colloids Surf. A Physicochem. Eng. Asp. 603 (2020), 125239, https://doi.org/10.1016/j.colsurfa.2020.125239.
[16] Q. Liu, X. Tan, S. Wang, F. Ma, H. Znad, Z. Shen, L. Liu, S. Liu, Environ. Sci. Nano. 6 (2019) 3158–3169, https://doi.org/10.1039/c9en00567f.
[17] Yang, Chem. Eng. J. 427 (2022), 131809, https://doi.org/10.1016/j.cej.2021.131809.
[18] A. Shahzad, K. Rasool, M. Nawaz, W. Miran, J. Jang, M. Moztahida, K. A. Mahmoud, D.S. Lee, Chem. Eng. J. 349 (2018) 748–755, https://doi.org/10.1016/j.cej.2018.05.148.
[19] A. Grzegórska, P. Głuchowski, J. Karczewski, J. Ryl, I. Wysocka, K. Siuzdak, G. Trykowski, K. Grochowska, A. Zielińska-Jurek, Chem. Eng. J. 426 (2021), https://doi.org/10.1016/j.cej.2021.130801.
[20] M. Kowalkińska, S. Dudziak, J. Karczewski, J. Ryl, G. Trykowski, A. Zielińska-Jurek, Chem. Eng. J. 404 (2021), 126493, https://doi.org/10.1016/j.cej.2020.126493.
[21] S. Weon, M.-J. Suh, C. Chu, D. Huang, E. Stavitski, J.-H. Kim, ACS EST Eng. 1 (2021) 512–522, https://doi.org/10.1021/acsestengg.0c00210.
[22] R. Katal, S. Masudy-Panah, M. Tanhaei, M.H.D.A. Farahani, H. Jiangyong, Chem. Eng. J., 384 (2020) 123384. doi.org/10.1016/j.cej.2019.123384.
[23] J. Yu, J. Low, W. Xiao, P. Zhou, M. Jaroniec, J. Am. Chem. Soc. 136 (2014) 8839, https://doi.org/10.1021/ja5044787.
[24] A. Gajewicz-Skretna, S. Kar, M. Piotrowska, J. Leszczynski, J. Cheminform., 13 (2021) 1–20. doi.org/10.1186/s13321–021-00484–5.
[25] A. Gajewicz-Skretna, A. Furuhama, H. Yamamoto, N. Suzuki, Chemosphere 280 (2021), 130681, https://doi.org/10.1016/j.chemosphere.2021.130681.
[26] P. Gramatica, QSAR Comb. Sci. 26 (26) (2007) 694–701, https://doi.org/10.1002/qsar.200610151.
[27] A. Tropsha, Mol. Inf. 29 (2010) 476–488, https://doi.org/10.1002/minf.201000061.
[28] N. Chirico, P. Gramatica, , J. Chem. Inf. Model. 51 (2011) 2320–2335, https://doi.org/10.1021/ci200211n.
[29] G. Li, K.A. Gray, Chem. Mater. 19 (2007) 1143–1146, https://doi.org/10.1021/cm061817f.
[30] H.A. Mahmoud, K. Narasimharao, T.T. Ali, K.M.S. Khalil, Nanoscale Res. Lett. 13 (2018), https://doi.org/10.1186/s11671-018-2465-x.
[31] F. Kong, X. He, Q. Liu, X. Qi, Y. Zheng, R. Wang, Y. Bai, Electrochim. Acta 265 (2018) 140–150, https://doi.org/10.1016/j.electacta.2018.01.196.
[32] A.A. Khan, M. Tahir, Ind. Eng. Chem. Res. 60 (2021) 16201–16223, https://doi.org/10.1021/acs.iecr.1c03242.
[33] X. Ding,Y. Li, C.Li, W. Wang, L. Wang, L. Feng, D. Han, J Mater. Sci., 54 (2019) 9385–9396. doi.org/10.1007/s10853–018-03289–4.
[34] I.A. Alsafari, S. Munir, S. Zulfiqar, M.S. Saif, M.F. Warsi, M. Shahid, Ceram. Int. 47 (2021) 28874–28883, doi.org/10.1016/j.ceramint.2021.07.048.
[35] D. Maarisetty, S.S. Baral, J. Mater. Chem. A 8 (2020) 18560–18604, https://doi.org/10.1039/d0ta04297h.
[36] T.X.H. Le, T.V. Nguyen, Z. Amadou Yacouba, L. Zoungrana, F. Avril, D.L. Nguyen, E. Petit, J. Mendret, V. Bonniol, M. Bechelany, S. Lacour, G. Lesage, M. Cretin, Chemosphere 172 (2017) 1–9, https://doi.org/10.1016/j.chemosphere.2016.12.060.
[37] M. Neamţu, M. Bobu, A. Kettrup, I. Siminiceanu, J. Environ. Sci. Health Toxic. Hazard. 48 (2013) 1264–1271, https://doi.org/10.1080/10934529.2013.776898.